



UNIVERSITEIT•STELLENBOSCH•UNIVERSITY
jou kennisvenoot • your knowledge partner

*Design procedure of a line-start permanent magnet synchronous machine
(repository copy)*

Article:

Sorgdrager, A.J., Grobler, A.J., Wang, R-J., (2014) Design procedure of a line-start permanent magnet synchronous machine, *Proc. of the Southern African Universities Power Engineering Conference*, (SAUPEC), Durban, South Africa, pp. 307--314, 30-31 January 2014

Reuse

Unless indicated otherwise, full text items are protected by copyright with all rights reserved. Archived content may only be used for academic research.

DESIGN PROCEDURE OF A LINE-START PERMANENT MAGNET SYNCHRONOUS MACHINE

A.J Sorgdrager^{*/**}, A.J Grobler^{**} and R-J Wang^{*}

^{*} Department of Electrical and Electronic Engineering, Stellenbosch University, Stellenbosch, South Africa

^{**} School of Electrical, Electronic and Computer Engineering, North-West University, Potchefstroom, South Africa

Abstract: This paper presents a method for designing an LS-PMSM by dividing the design into sub-machine components. Each of the individual sub-machine components is then designed using several classical machine design principles. Once all the components have been designed they can be combined to form an LS-PMSM. The machine design is verified in two manners. Firstly the selected flux density values are compared with the FEM values to ensure they are in range of each other. Secondly the calculated asynchronous and synchronous performance is compared with the simulation results from a commercial design software package. Finally the proposed method is applied to the design of a prototype machine. The results show a good agreement with that obtained from commercial design package.

Key Words. LS-PSMS; permanent magnet synchronous motor; line-start; machine design.

1. INTRODUCTION

Induction machines (IM) are the backbone of the industry machine installation as they are robust, reliable and have relatively high efficiency. In a typical South African chemical plant the majority of electrical machines are IMs ranging between 2.2 kW and 22 kW. The majority of the machines in this power range are connected to pump and fan loads. Both of these load types are operated at a constant speed. As the price of electrical energy increases and stricter efficiency regulations are implemented in place, there is a need for more efficient electrical machines.

In 2008 the International Electro-technical Committee (IEC) standardized the efficiency classes for three-phase, line-fed general purpose machines to promote a market transformation [1]. The IE4 (Super-premium efficiency) is the highest of the four standards and was initially only intended to be informative. Many machine manufacturers saw no possibility of reaching these efficiency levels with IMs within the respective IEC frames [1]. This forced the manufacturers to investigate other technologies like permanent magnet synchronous machines (PMSM). The problem with a PMSM is that it is not self-starting thus limiting the possibility of acting as a direct replacement of an IM.

In 1971, Binns et. al. proposed a new type of self-starting synchronous machine that utilized both permanent magnets (PM) and a die-cast cage within a single stack of laminations [2]. The cage generates asynchronous torque during transient operation, which makes it possible for the machine to be started directly from the ac supply. This machine type is now known as a line-start permanent magnet synchronous machine (LS-PMSM).

In theory an LS-PMSM is a hybrid of a PMSM and an IM in a single rotor. During the transient period the asynchronous torque (T_{asy}) is the result of the interaction between the cage torque (T_c) and breaking torque (T_m) [3]. Both the breaking torque and the cage torque are dependent on different component in the

machine. T_m is generated by the PM and has a negative effect on the machine's start-up performance. The magnitude of this negative torque component is dependent on the PM volume [4, 5]. At steady state, the synchronous torque (T_{syn}) is mainly produced by the PM alignment torque. Depending on the rotor topology there can also be a reluctance torque component. The performance of the machine is greatly influenced by the interaction between the IM and PMSM topology [3,5]. Once the rotor is synchronized with the stator's rotating MMF, the rotor cage has no effect on torque production. This eliminates the cage rotor losses of the machine at steady state because there are no induced currents in the bars. Thus the efficiency of an LS-PMSM can be higher than that of an IM [3]. Figure 1 illustrates the torque components of a generic LS PMSM.

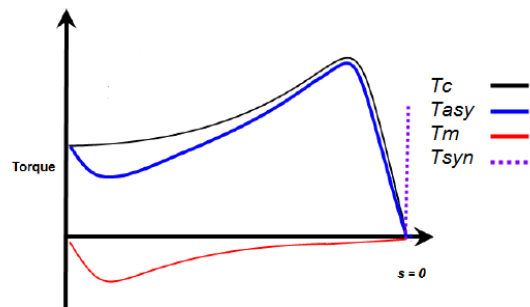


Figure 1: LS PMSM theoretical torque curves [3, 6]

Several comparison studies between IMs and LS PMSMs have been done during the last couple of years. In [7], it is concluded that an LS-PMSM has superior performance when compared to an IM with regards to pump, fan and compressor loads (constant speed with long operating cycle loads). Typically an LS-PMSM has higher efficiency, power factor and torque density and its operating temperature is lower than that of an IM due to the absence of rotor bar currents [1,7-9]. Although these machines' initial cost is higher than that of an IM, the cost of ownership is much less, making it a very suitable machine for certain applications. The drawback of this machine is however its starting torque and synchronisation capabilities, which place limits on its application capabilities.

This paper presents a design methodology for LS-PMSM, which utilizes classical machine design theory in combination with finite element method (FEM) analysis. The proposed method is applied to the design of a four-pole, low voltage LS-PMSM driving a fan-type load.

2. PROPOSED DESIGN METHOD

When designing an LS-PMSM there are two options available. The most popular one found in literature is a retro-fit design or IM rotor swop-out [6]. Since an LS-PMSM can operate with the same stator as an IM the IM rotor can be replaced with an LS-PMSM rotor [3, 4, 9, 10]. This option eliminates the need of machine sizing. The second option is to do a complete machine design. The method proposed in this paper can be used for both options. For the retrofit option the stator must be characterised instead of designed but the same steps must be followed as some of the stator parameters are needed during the rotor design.

Figure 2 shows the low-level design flow diagram. The black dashed lines represents the need for changes in the design should the relevant parameters and flux density's not be met during the FEM verifications. Each of the four blocks is an independent sub-design for a component of the machine. As the rotor contains both an IM and a PMSM, they can be designed separately. Once both rotor designs are done they can be combined into one rotor. The PMSM is designed first as the magnetic braking torque must be known to design the cage torque curve. During the design of the PMSM the possible cage location must be kept in mind.

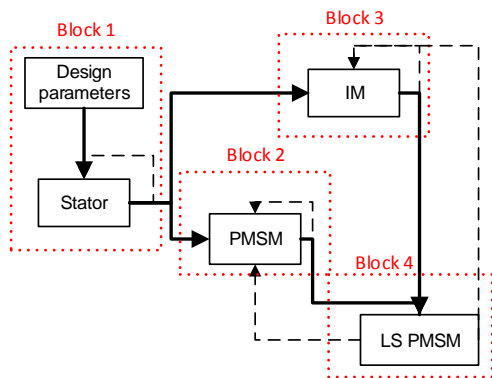


Figure 2: LS PMSM design processes

Figure 3 contains the design steps of Block 1. This block has a 2-step design: in the first step the machine is sized to determine rotor diameter (D_r) and active length (l). In the second step the winding factor (k_w), turns per coil (N_s) and the coil slot is determined. This design method was adapted and compiled from [10] and [11].

Once the stator design is complete the design must be verified to determine if the selected flux density values are achieved. This is done through static FEM analysis. The PMSM (Block 2) and IM (Block 3) design flow diagrams are shown in Figure 4 and 5,

respectively. Both Block 2 and 3 was compiled using [10 – 12].

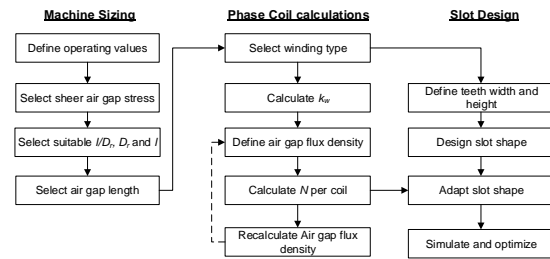


Figure 3: Design flow diagram of Block 1 [6]

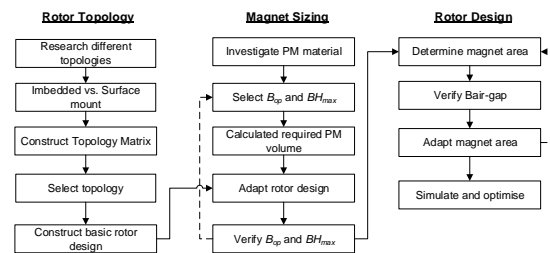


Figure 4: Design flow diagram of Block 2 [6].

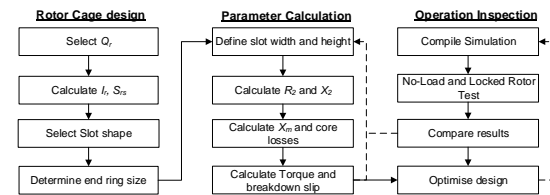


Figure 5: Design flow diagram of Block 3 [6].

Once both the PMSM and IM rotors sections have been designed and verified the two must be combined to form the LS-PMSM rotor. The performance of the LS-PMSM can then be compared to the two independent machines. Theoretically state the LS-PMSM's performance will be similar to that of the PMSM and during transient operations to the IM although there will be difference due to the presence of T_m . For the static FEM simulations FEMM is used and for the performance comparison with the calculated model, Maxwell[®] RMXprt is used.

3. DESIGN AND VERIFICATION

In this section the afore-proposed method is implemented in the design of a prototype LS-PMSM machine.

3.1 Design Specifications

Table 1 contains the design specifications of the prototype machine. Besides the specifications in Table 1, the starting current of the machine is required to be similar to that of an IM with the same power rating. Furthermore the prototype must fit in a

132 size frame or smaller, enabling the machine to be used as a direct replacement for an existing IM.

Table 1: Prototype Machine Specifications

Specification	Value
Power (kW)	7.5
Phase	3
Line Voltage (V)	525
Line Current (A)	± 10
Number of Poles	4
Preferred Line Connection	Star
Rated Speed (RPM)	1500
Duty Cycle	S1

3.2 Machine Sizing

To determine l and D_r , two options are available. The first option is to use the values of the IM counterpart and change either l or D_r while the second option varies both parameters. In both options (1) is used

$$\begin{aligned} T_{rated} &= \sigma r_r S_r \\ T_{rated} &= \sigma r_r (2\pi r_r l) \\ T_{rated} &= \frac{\sigma \pi D_r^2 l}{2} \\ \sigma &= \frac{2T_{rated}}{\pi D_r^2 l} \end{aligned} \quad (1)$$

with T_{rated} being the rated torque of the machine and σ the tangential stress or sheer air-gap stress of the machine [10]. The tangential stress is the main torque producing component when it acts on the rotor surface. If σ is selected to be within limits as set out in [6] only the l and D_r is unknown. By fixing one of the two unknown and performing a variable sweep the other can be selected out of the graph. The selected value is then re-checked by fixing the selected value and performing a sweep again. A graph similar to Figure 6 can then be compiled. The l/D_r ratio must be checked to aid in final selection with the empirical ratio rule i.e.

$$\begin{aligned} X &\approx \frac{l}{D_r} \\ X &= \frac{\pi}{2p} \sqrt[3]{p} \\ X &= 1 \end{aligned} \quad (2)$$

with p being the number of pole pairs [10]. The rotor diameter D_r must not be selected too small as this complicates the rotor design and limits the cross sectional area. The values of l and D_r for the design is 115 mm and 113.5 mm respectively. The air-gap (δ) length is selected as 0.5 mm.

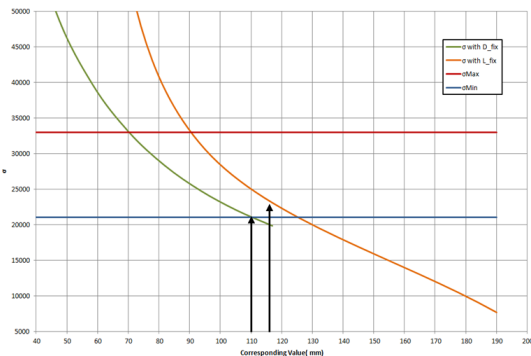


Figure 6: Variable sweep of LS PMSM design

3.3 Stator Design

Once the machine is sized the next step is to determine the winding factor (k_w), number of turns per coil phase (N_s) and the required slot area. To do this, the air gap flux density (B_δ) must be selected. For a PMSM the value of B_δ is usually between 0.85-1.05 T depending on the rotor topology, as for an IM the values is between 0.7-0.9 T [10]. By selecting the value as 0.85 T both machine's boundaries are respected.

In [6], a harmonic comparison study was done to select the winding layout. A 36 slot, overlapping double-layer layout was selected as it provided the best slot harmonics of the options. The coils are short pitched by one slot. Table 2 contains the winding configurations that were investigated with Q_s as the number of slots, q the number of slots per pole per phase, k_d the distribution factor, k_p the pitch factor and k_{sq} the skewing factor.

Table 2: Compilation of Various Winding Factors [6]

Q_s	q	k_d	k_p	k_{sq}	k_w
24	2	0.9659	1	0.9886	0.9549
24	2	0.9659	0.9659	0.9886	0.9223
36	3	0.9597	1	0.9949	0.9548
36	3	0.9597	0.9848	0.9949	0.9403
48	4	0.9576	1	0.9971	0.9548
48	4	0.9576	0.9914	0.9971	0.9466

As it is very difficult to skew the rotor bars and PM with respect to the stator it was decided to skew the stator slots by one slot pitch instead. This technique is not that common in mass produced IMs but is used in specific cases.

To calculate N_s , k_w is used in

$$\begin{aligned} N_s &= \frac{\sqrt{2}E_m}{\omega_e k_{w1} \Phi_m} \\ N_s &= \frac{\sqrt{2}E_m}{\omega_e k_{w1} (\alpha_{pa} B_\delta \tau_p l')} \end{aligned} \quad (3)$$

with Φ_m being the PM flux [10]. Note the expansion of Φ_m in (3), where the air gap flux density B_δ and pole area is used. Table 3 contains the values and the definition of each symbol in (3). The pole arch coefficient is dependent on the rotor topology and seldom exceeds 0.85. The actual value can only be calculated once the final rotor has been designed.

Table 3: Values for Calculations of N_s

Symbol	Value	Description
E_m	303V	Phase voltage
ω_e	100π rad/s	Electrical angular velocity
k_{w1}	0.9403	Winding factor
α_{ac}	0.8	Pole arch coefficient
B_δ	0.85 T	Air gap flux density
τ_p	0.089 m	Pole pitch
l'	0.115 m	Active length

Using the values listed in Table 3, N_s is calculated as 208. This value is rounded to 216 to provide 36 turns per slot. When substituting this value into (3), B_δ is recalculated as 0.868 T which is an acceptable increase of less than 3%.

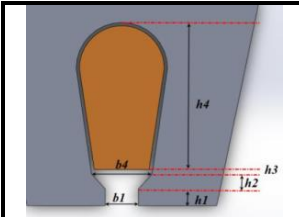
The required slot size can be calculated using N_s , the wire's copper area and the fill factor (ff). The rated current is calculated as 10A. The stator coil current density (J_s) must be selected to calculate the required size of copper wire [10]. By selecting J_s as 6.5 A/mm² the required copper area per conductor is ± 1.6 mm² thus a SWG17 (1.422 mm \varnothing) can be used. However to gain a better fill factor, two SWG19 (1 mm \varnothing) is used. By doing so, J_s is re-calculated as 6.3 A/mm². Thus a single slot contains 72 conductors with a copper area of 60 mm². For the LS-PMSM the fill factor is selected as 0.5, thus the required slot area is 120 mm². To further aid in designing the slot shape the stator slot height (h_s) and tooth width (b_{st}) is calculated by selecting the flux density values in the teeth and back yoke as set in [6]. Table 4 contains the selected flux density values and calculated values of h_s and b_{st} . The tooth flux density is at its maximum on the d-axis and gradually decreases towards the q-axis. Thus the value in Table 4 is the peak value and not the average value.

As indicated in Figure 3, once h_s and b_{st} is calculated the slot shape must be selected and optimized. The final slot shapes parameters are listed in Table 5. Once the design is finalised the stator parameters (stator winding resistance (R_1) and the reactance (X_1)) can be calculated. R_1 is calculated using the combined method of [10] and [13]. Table 6 contains R_1 and the relevant performance factors (λ – not to be mistaken for flux linkage) used to calculate the stator leakage reactance. The leakage effects of skewing can only be incorporated once the initial inductance is calculated [10].

Table 4: Stator Slot Height and Width Parameters

	Yoke	Tooth
B (T)	1.4	1.7
h_t & b_{st} (mm)	35.5	4.5

Table 5: Stator slot dimensions



	mm
b_1	2.4
b_4	4.2
h_1	1.3
h_2	1.3
h_3	0.5
h_4	26.5

Table 6: Calculated Stator Parameters.

Parameter	Value
R_1	1.40544 Ω
Slot leakage (λ_{sl})	2.8836 Wb
End winding leakage (λ_{sw})	0.24197 Wb
Zig-zag leakage (λ_{szz})	0.1785 Wb
X_1 without skewing	2.343 Ω
Skew leakage (L_{ssq})	75.424 μ H
X_1	2.3668 Ω

To verify the stator design, the selected flux density values in both the stator yoke and teeth will be compared to the results from the FEM simulation model to check if they are in a good agreement. A simple surface-mounted PM rotor that generates $B_\delta = 0.85$ T may be used to verify the stator design as shown in Figure 7. A full pitch surface mount PMSM

is used as the flux density values of the PM is the flux density value of the air-gap. Thus by setting remanence value of the magnet to 0.85 T, the correct B_δ is obtained for verification. Model A is between two d-axes and Model B between two q-axes. The stator coils in both models are not excited. The simulation results of both models are listed in Table 7. The calculated value differs from that selected values in Table 4 as both the slot height and width was reduced during the slot optimization. M400-50A lamination material is used for the stator.

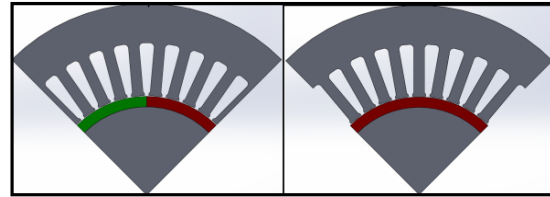


Figure 7: Stator verification models

Table 7: Stator Verification Information

	Stator Yoke Flux Density	
	FEM	Calculated
Model A	1.337 T	1.22 T
Model B	1.383 T	
	Stator Teeth Flux Density	
	FEM	Calculated
Model A	1.206 T	1.3 T
Model B	1.33 T	

From the table it can be seen that the calculated flux density values correlate with the FEM simulated ones.

3.4 Rotor Design

As indicated by Figure 2 the rotor design comprises of two parts. The PMSM rotor is designed first to simplify the design process as the PMs influence the space availability of the rotor the most. Furthermore the breaking torque must be known in order to design the cage to overcome it.

3.4.1 PMSM Rotor Component

Although many rotor topologies of PMSM exists, this study only considers four topologies namely surface mount magnets (SMM), slotted surface mount magnets (SSMM), imbedded radial flux magnets (IRFM) and imbedded circumferential flux magnets (ICFM) as shown in Figure 8.

Surface mounted topologies (SMM and SSMM) exhibit good steady-state performance, but suffer from poor transient operation capabilities [6]. Imbedded radial flux topology leads to high magnet consumption [6,14]. Thus the ICFM topology was selected as it provides the highest B_δ in comparison with the other 3 topologies for the same PM volume [14]. The key design consideration of ICFM topology is the large leakage flux through the shaft. This can be greatly reduced by using a non-magnetic shaft material.

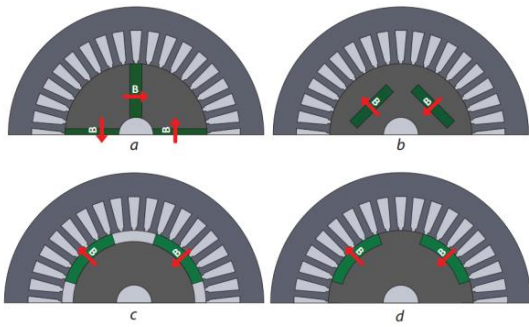


Figure 8: PM rotor topologies: a) ICFM; b) IRFM; c) SMM and d) SSMM [6, 14]

To determine the minimum PM volume to provide an airgap flux density of 0.85 T the assumption was made that there is no leakage flux in the rotor, thus $\Phi_m = \Phi_\delta$ and the PM volume (Vol_m) can be calculated with

$$Vol_m = \frac{Vol_\delta B_\delta^2}{\mu_0 (-H_m B_m)} \quad (3)$$

with Vol_δ the air gap volume and $H_m B_m$ the energy product of the operation point of the magnet [12]. By replacing $H_m B_m$ with the HB_{max} value of the selected PM grade, the magnet provided the maximum magnetic energy per material volume. As the active length of the machine is known only the height and thickness of the magnet must be selected. To provide adequate space for the cage the magnet height was selected as 26 mm. Table 8 contains the magnet thicknesses (t_m) as calculated with (3) for different PM grades.

Table 8: PM Thickness Sizing for Different Grades

Grade	N42	N40	N38	N35	N33	N30
t_m (mm)	3.1	3.24	3.78	3.9	4.2	4.57

All the magnets in Table 8 provide the same B_δ as ICFM utilizes flux concentration to form the poles [6]. It was decided to use a N33 grade PM and to increase the thickness to 6mm to accommodate for loss in magnetic energy due to leakage flux. Figure 9 indicates that the selected magnet volume provides the required energy (red line) at both rated (blue line) and operating (green line) temperature. The intersection points are the operation point of the magnets. The selected PM dimensions provided the required B_δ value.

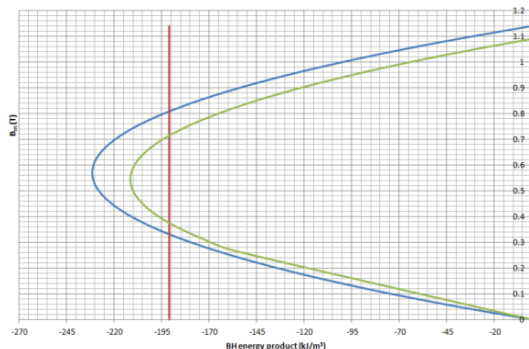


Figure 9: BH energy plot of the selected PM grade

The synchronous torque (T_{syn}) of the PMSM is the sum of electromagnetic torque (T_{em}) and reluctance torque (T_{rel}) components and is calculated using the general torque equation for a PMSM. The torque vs. load angle curve for the PMSM is indicated Figure 10. The values used to plot Figure 10 is d -axis reactance, $X_d = 29.329 \Omega$, q -axis reactance, $X_q = 85.841 \Omega$ and back-EMF, $E_0 = 186.362$ V. These values were calculated as in [10] and [16].

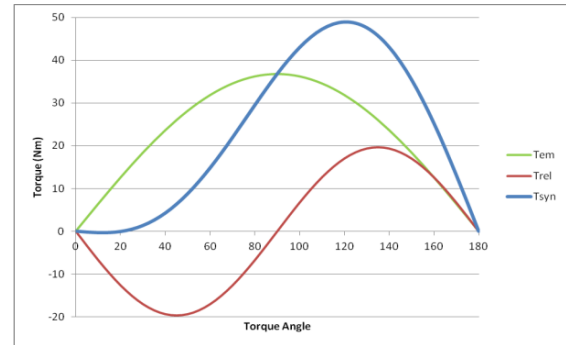


Figure 10: PMSM torque vs. load angle curve.

The breaking torque in an LS-PMSM was first investigated in 1980 by V.B Honsinger and published in his well-known paper [15]. T_m is calculated as a function of slip with (4). Figure 11 contains T_m 's plot with a peak value of ± 14 N.m at $s = 0.045$.

$$T_m = \frac{3p}{\omega(1-s)} \left[\frac{R_1^2 + X_q^2(1-s)^2}{R_1^2 + X_q X_d(1-s)^2} \right] \left[\frac{R_1 E_o^2(1-s)^2}{R_1^2 + X_q X_d(1-s)^2} \right] \quad (4)$$

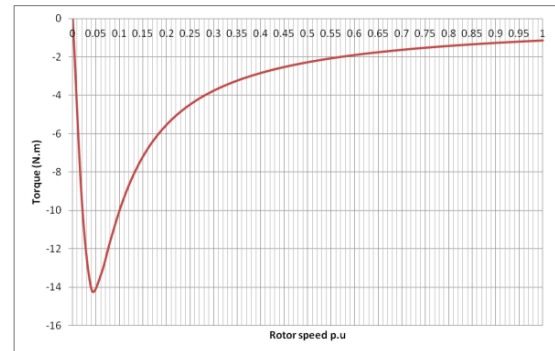


Figure 11: Breaking torque component of the PMSM in the LS PMSM prototype

3.4.2 IM Rotor Component

The first step in the IM design is to select the number of rotor slots (Q_r). As a slot is required above each PM to limit the leakage flux Q_r must be divided by four. For the prototype rotor Q_r is selected as 24 with information gained from [10] and [11]. For ease of manufacturing round rotor slots will be used.

As with the stator the rotor yoke and tooth flux density must be selected to calculate the slot height and width. As the PM span the rotor yoke, the remanence value of the PM is used. This provided a yoke height of 26.63 mm. The maximum tooth flux density occurs on the d -axis and gradually decreases between each tooth towards the q -axis. By selecting the maximum value of 2.2 T the tooth width is

calculated as 7.425 mm. The next step is to determine the remaining dimensions of the round slot as in Figure 12. This is done with the aid of the slot performance factor (λ_{ru}) equation that directly influences the rotor inductance (L_2). By minimizing λ_{ru} , L_2 is also minimized. λ_{ru} is calculated with (5). The most influential dimension is the slot opening (b_1). Increasing the slot opening area will reduce the leakage flux whereas a deep slot will increase it. The values for b_1 and h_1 are selected as 2 mm and 1 mm respectively which results in $\lambda_{ru} = 3.078$. Along with λ_{ru} , the end ring performance factor (λ_{rer}), must be determined before L_2 can be calculated. The dimensions of the end rings were determined as 12 mm by 12 mm providing $\lambda_{rer} = 0.37007$.

$$\lambda_{ru} = 0.47 + 0.66 \frac{b_4}{b_1} + \frac{h_1}{b_1} \quad (5)$$

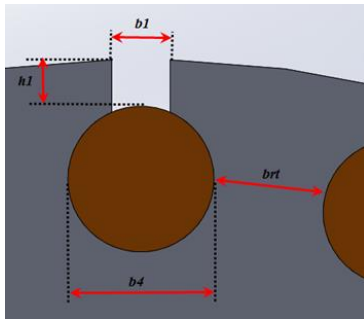


Figure 12: Rotor slot dimensions

To calculate R_2 , the rotor bar and end-ring resistance must be calculated, these values are calculated as 99 $\mu\Omega$ and 3.53 $\mu\Omega$ respectively as in [10, 11]. Once R_2 and L_2 is calculated in rotor reference frame these value must be transformed to the stator reference frame. The transformed values are $R_2' = 2.187 \Omega$ and $X_2' = 1.615 \Omega$ with X_2' being the rotor reactance in the stator reference frame.

With the aid of the machine parameters the starting and breakdown torque can be calculated. Both of these torque values are a function of the starting current. Table 9 contains the relevant torque and current values. The torque vs. slip curve will be provided in Section 5.

Table 9: Starting and Breakdown Parameters

Parameter	Symbol	Value
Starting Current	T_{start}	55.93 A
Starting Torque	T_{start}	130.67 N.m
Breakdown Torque	T_{bd}	153.59 N.m
T_{db} slip speed	s_{db}	0.511

3.4.3 LS-PMSM

Now that both the PMSM and IM rotor components have been designed the next step is to combine the two to form the design of LS-PMSM prototype rotor as shown in Figure 13. To ensure that a single lamination can be used two saturation zones are use between the PM and shaft as well as the PM and rotor bar. The original gap between the rotor bar and PM was 1.425 mm. However the PM leakage flux as determined from static FEM simulations was 18% of

the total PM flux. By increasing the shaft diameter with 1 mm the gap was reduced to 0.952 mm resulting in a 10% PM leakage flux which is acceptable according to the PM sizing done in 4.3.1.

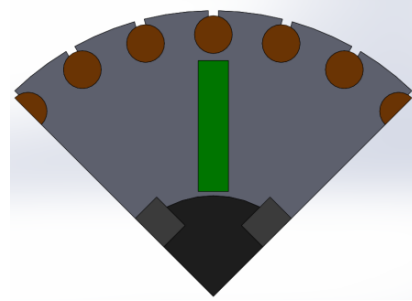


Figure 13: Quarter section of LS-PMSM Rotor

To verify the LS PMSM rotor the air gap flux, rotor yoke and teeth flux density will be used. For the FEM simulation the machine is driven a full load line current ($I_{line} = 10A$) at synchronous speed, Δf between the rotor and stator is zero. Table 10 shows the verification results. The tooth flux density is checked on the d -axis between two teeth.

Next, the air gap flux density of the machine is verified. The air gap flux density plot is taken over the pole arch and not the pole pitch as the flux only passes the air gap over the pole arch. If the flux over the pole is used a lower average flux density value will be obtained. The average flux density over the pole arch is calculated as 0.84 T which is acceptable. Thus the conclusion can be made that the simulation model is an accurate representation model of the LS PMSM machine.

Table 10: LSPMSM Rotor Verification Information

	Rotor Yoke Flux Density		
	FEM	Calculated	% Difference
Tooth 1	2.29 T	2.2 T	4
Tooth 2	2.082 T		6
	Rotor Teeth Flux Density		
	FEM	Calculated	% Difference
	1.208 T	1.17 T	3.2

4. PERFORMANCE PREDICTIONS AND SIMULATIONS

In this section the torque profile and the back-EMF properties of the prototype will be investigated. The calculated and simulation results of the asynchronous and synchronous torque components will be compared. This is done to ensure that the method used to design the prototype is correct. The back-EMF peak value is calculated and determined from the FEMM model. The peak back-EMF value is a key component in calculating the breaking torque of any LS-PMSM.

4.1 Asynchronous Torque Profile

In initial comparisons it was found that ignoring the skin effect on the rotor bars provided a significant

error in torque calculations. Once the effect was incorporated into the design the simulated and calculated torque curves are within acceptable range. Figures 14 provide a comparison between the cage torque with and without the skin effect while Figure 15 contains the revised T_{asy} curve and its components. The comparison between the calculated and simulated T_{asy} curves is given in Figure 16. The simulated results were obtained by using Maxwell[®] RMxpirt.

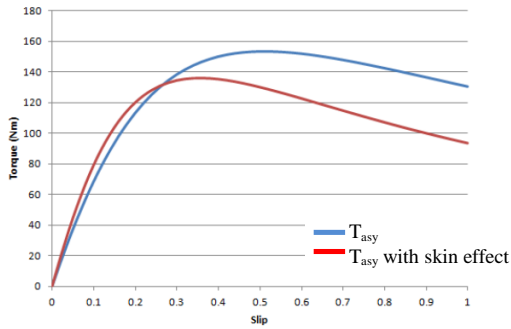


Figure 14: Cage torque with and without skin effect

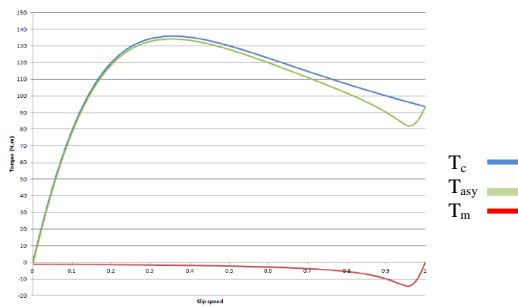


Figure 15: Torque vs. slip of different torque components (including skin effect)

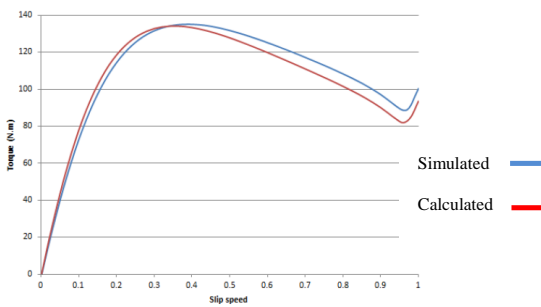


Figure 16: Simulated torque curve vs. calculated torque curve

Table 11: Simulation vs. Calculated Starting and Breakdown Results.

	Calculated	Simulated	% Difference
I_{start}	52.37 A	52.84 A	< 1 %
T_{start}	93.604 N.m	100.94 N.m	7.2 %
T_{bd}	136.01 N.m	135.20 N.m	0.5 %
s_{bd}	0.356	0.4	11%

Table 11 contains the breakdown and starting values for both the simulated and calculated machine.

4.2 Synchronous Torque Profile

The last comparison between the proposed model and the Maxwell RMxpirt model is the torque versus load angle plot as indicated in Figure 17. The maximum

calculated torque is 48.9 N.m at $\delta = 120^\circ$ and the simulated maximum torque is 48.39 N.m at $\delta = 119^\circ$. Both the maximum torque and angle are within range of each other.

Table 12 contains the simulated and calculated parameters. The skin effect is included in the calculated parameters as the RMxpirt simulation also incorporates the skin effect, thus providing an accurate resistance and inductance comparison.

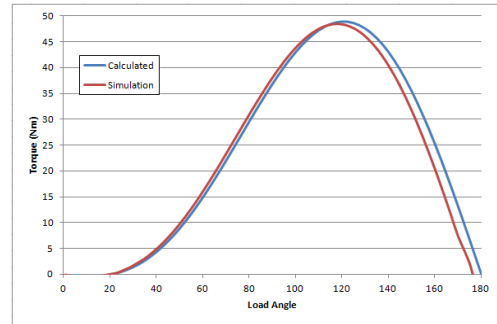


Figure 17: Load angle of simulated torque vs. calculated torque

Table 12: Parameter Comparison

	Proposed Method	Maxwell RMxpirt	% Difference
R_l	1.428	1.423	< 1 %
R_2'	1.787	1.679	6 %
X_l	2.387	3.02	26 %
X_2'	1.6473	1.802	9.3 %

All the parameters except for X_l are within 10%, the effect of changing this value so that it is within 10% of the calculated value is investigated. By reducing the X_l the T_{start} and I_{start} increases. Thus the conclusion can be that the simulation package uses a different method to calculate the starting and breakdown values.

4.3 Back-EMF

The back-EMF of an LS-PMSM is a function of the PM flux linkage (λ_{pm}) with the stator coil phases with respect to the rotational speed of the rotor. The flux linkage of each phase is calculated in FEMM, by setting the phase current's value to zero. This simulates the rotor rotating at synchronous speed. To calculate the peak back-EMF value one of the phases must be aligned with the rotor d-axis. Once the flux linkage value of each phase is extracted the RMS back-EMF value is calculated as 186.167 V. This value correlates with the RMS phase back-EMF value calculated in ANSYS Maxwell[®] as 190.19 V.

5. CONCLUSION

The design method presented in this paper proved to present an adequate fit to the simulated results as indicated in Section 4. An efficient design approach for LS-PMSM has been presented in the paper. By dividing the LS-PMSM rotor design into two separate designs i.e. IM and PMSM, the final rotor's performance can be readily represented by using

classical electrical machine theory. To validate the proposed design approach, the calculated results are compared with the simulation results from both a FEM and a commercial design package. A good agreement is achieved.

During the initial design of the cage the skin effects was neglected, which caused a poor match between the calculated and simulated cage torque curves. Once the skin effect was incorporated the two torque curves correlated well. In future designs this effect must be incorporated in the design.

The calculated stator reactance differed greatly from the simulated value. Investigation into other calculation methods must be done and compared with the current method to refine the calculation of this parameter. Once this is done the proposed method in this paper can be seen as a viable design tool.

REFERENCES

- [1] T A de Almeida, F J Ferreira, and J A Fong, "Standards for efficiency of electrical motors," *IEEE Industry Applications Magazine*, vol. 17, no. 1, pp. 12-19, Jan/Feb 2011.
- [2] K.J Binns, W.R Barnard, "Novel design of self-strating synchronous motor", *Proceedings of the Institution of Electrical Engineering*, vol. 118, no 2 Feb 1971.
- [3] P W Hung, S H Mao, and M C Tsai, "Investigation of line start permanent magnet synchronous motors with interior-magnet rotors and surface-magnet rotors," *Electrical Machines and Systems*, pp. 2888 - 2893, October 2008.
- [4] A.H Isfahani, "Effects of magnetizing inductance on start-up and synchronization of line-start permanent-magnet synchronous motors," *IEEE Transaction on magnetics*, vol. 47, no. 4, pp. 823-829, April 2011.
- [5] F.J.K Kalluf, "Braking torque analysis of the single phase line-start permanent magnet synchronous motor," in *XIX Intenational conference on electrical machines*, Rome, 2010.
- [6] A.J Sorgdrager, "Development of a line-start permanent-magnet synchronous machine", Master thesis, North-West University: Potchefstroom, 2013
- [7] A.H Isfahani, S Vaez-Zedeh "Line start permanant magnet synchronous motors: challenges and opportunities," *Elsevier: Energy*, vol. 34, pp. 1755-1763, April 2009.
- [8] C. Mutize, R-J. Wang, "Performanse comparison of an induction machine and line-start PM motor for cooling fan applications," in *Proceedings of the 21st Southern African Universities Power Engineering Conference, (SAUPEC)*, 2013, pp.122-126.
- [9] L Weili, Z Xiaochen, and C Skukang, "Study of solid rotor line-start PMSM operating performance," in *International Conference on Electrical Machines and Systems*, 2008, pp. 373-378.
- [10] J Pyrhonen, *Design of rotating electrical machines*, 1st ed. West Sussex, United Kingdom: John Wiley & Sons, Ltd, 2008.
- [11] I Boldea, *Electric machines*, 1st ed. USA: CRC Press, 2010.
- [12] A.E Fitzgerald, *Electrical machinery*, 6th ed. New Yourk, USA: Mc Graw Hill, 2003.
- [13] I Boldea, *The induction machine handbook*, 1st ed. New York, USA: CRC Press, 2002.
- [14] A.J Sorgdrager, A.J Grobler, "Influence of Magnet Size onf the Air-gap Flux Density of n Radial Flux PMSM." IEEE International Conference on Industrial Technology, Cape Town, 2013, 337-343.
- [15] V.B Honsinger, "Permanent magnet machines: Asynchronous operation," *IEEE Transactions on Power Apparatus and Systems*, vol. PAS-99, no. 4, pp. 1503-1509, July 1980.
- [16] D Henselman, *Brushless permanet magnet motor design*, 2nd ed. Orono, USA: Magna physics publishing, 2006.